

# SYMPLECTIC METHODS IN SPACE MISSION DESIGN

Cengiz Aydin,<sup>\*</sup> Urs Frauenfelder,<sup>†</sup> Dayung Koh <sup>‡</sup> and Agustin Moreno <sup>§</sup>

Using methods from symplectic geometry, the second and fourth authors have provided theoretical groundwork and tools aimed at analyzing periodic orbits, their stability and their bifurcations in families, for the purpose of space mission design.<sup>1</sup> The Broucke stability diagram<sup>2</sup> was refined, and the "Floer numerical invariants" were considered, as numbers which stay invariant before and after a bifurcation, and therefore serve as tests for the algorithms used, as well as being easy to implement. These tools were further employed for numerical studies.<sup>3</sup> In this article, we will further illustrate these methods with numerical studies of families of orbits for the Jupiter-Europa system, with emphasis on planar-to-spatial bifurcations, from deformation of the families in Hill's lunar problem studied by the first author.<sup>4</sup>

## INTRODUCTION

Symplectic geometry is the branch of mathematics that studies the geometric properties of phase spaces, those spaces that describe the possible states of a classical physical system. It provides the proper framework in order to address problems in classical mechanics, e.g., the gravitational problem of  $N$  bodies in three-dimensional space. In the last thirty years, a host of theoretical tools have been developed in the field, with *Floer theory* as a notable example, whose emphasis is on the theoretical study of periodic orbits. In a more applied direction, periodic orbits are of interest for space mission design, as they model trajectories for spacecraft or satellites. Studying families of orbits aimed at placing a spacecraft around a target moon is relevant for space exploration, where optimizing over all possible trajectories is needed, in order to minimize fuel consumption, avoid collisions, and maximize safety. In this context, the influence on a satellite of a planet with an orbiting moon can be approximated by a three-body problem of *restricted* type (i.e., the mass of the satellite is considered negligible by comparison). This is a classical problem which has been central to the development of symplectic geometry, and therefore it is not unreasonable to expect the modern available tools to provide insights. The need of organizing all information pertaining to orbits leads to the realm of data analysis, for which computationally cheap methods are important. The direction we will pursue is then encapsulated in the following questions:

<sup>\*</sup>PhD, Institut de mathématiques, Université de Neuchâtel, Switzerland, cengiz.aydin@hotmail.de

<sup>†</sup>Prof. Dr., Institut für Mathematik, Augsburg Universität, Germany, urs.frauenfelder@math.uni-augsburg.de

<sup>‡</sup>dayung.koh@gmail.com

<sup>§</sup>JProf. Dr., Universität Heidelberg, Germany, agustin.moreno2191@gmail.com

## Guiding questions

- **(Classification)** Can we tell when two orbits are *qualitatively different*<sup>a</sup>?
- **(Catalogue)** Can we resource-efficiently refine data bases of known orbits?
- **(Symplectic geometry)** Can we use methods from symplectic geometry to guide/organize the numerical work?

---

<sup>a</sup>We say that two orbits are *qualitatively different* if they cannot be joined by a regular family of orbits.

The first two questions were addressed by the second and fourth authors, where the mathematical groundwork is explained.<sup>1</sup> The second, third, and fourth authors used it in combination with numerical work, addressing the third question.<sup>3</sup> In this article, we continue this line of research. We have the following tools at our disposal.

## Toolkit

- (1) **Floer numerical invariants:** Numbers which stay invariant before and after a bifurcation, and so can help predict the existence of orbits, as well as being easy to implement. There is one invariant for arbitrary periodic orbits, and another for *symmetric* periodic orbits.<sup>3</sup>
- (2) **The B-signs:**<sup>1</sup> a  $\pm$  sign associated to each elliptic or hyperbolic Floquet multiplier of an orbit<sup>a</sup>, which helps predict bifurcations. This is generalization of the classical Moser–Krein signature,<sup>5–7</sup> which originally applies only to elliptic Floquet multipliers, to also include the case of hyperbolic multipliers, whenever the corresponding orbit is *symmetric*.
- (3) **Global topological methods:** the *GIT-sequence*,<sup>1</sup> a sequence of spaces whose global topology encodes (and sometimes forces) bifurcations, and refines Broucke’s stability diagram<sup>2</sup> by adding the *B*-signs.
- (4) **Conley-Zehnder index:**<sup>8,9</sup> a winding number associated to each non-degenerate orbit, extracted from the topology of the symplectic group, which does not change unless a bifurcation occurs. Therefore it can be used to determine which families connect to which.

---

<sup>a</sup>Recall that the Floquet multipliers of a closed orbit are by definition the non-trivial eigenvalues of the monodromy matrix.

Combining the Floer numbers with the *B*-signs provides tools to decide whether to look for periodic orbits, and gives hints concerning where to actually look for them. In this paper, we apply these tools in numerical studies of families of periodic orbits in the Jupiter-Europa system, by deformation of families in the lunar problem studied by the first author.<sup>4</sup> Our results illustrate the general principle that one may learn about a given system, by starting from known nearby systems, and then deforming. The main result is a bifurcation graph relating various families (Figure 14), including a *spatial* family connecting two *planar* orbits, one retrograde, and the other, prograde; it may then be used in practice to visit the poles. Our novel tools were instrumental for our results.

## PRELIMINARIES

In this section, we review the toolkit. But first, we set up some language and notation.

### Basic notions

**Mechanics/symplectic geometry.** Given a  $2n$ -dimensional phase-space  $M$  with its symplectic form  $\omega$ , a Hamiltonian function  $H : M \rightarrow \mathbb{R}$ , with Hamiltonian flow  $\phi_t^H : M \rightarrow M$  which preserves  $\omega$  (i.e.  $(\phi_t^H)^*\omega = \omega$ ), and a periodic orbit  $x$ , the *monodromy matrix* of  $x$  is  $M_x = D\phi_T^H$ , where  $T$  is the period of  $x$ . Then  $M_x$  is a symplectic  $2n \times 2n$ -matrix; we denote by  $Sp(2n)$  the space of such matrices (the *symplectic group*).

Note that if  $H$  is time-independent then 1 appears twice as a *trivial* eigenvalue of  $M_x$ . We can ignore these if we consider the *reduced* monodromy matrix  $M_x^{red} \in Sp(2n-2)$ , obtained by fixing the energy and dropping the direction of the flow.

- A *Floquet multiplier* of  $x$  is an eigenvalue of  $M_x$ , which is not one of the trivial eigenvalues (i.e. an eigenvalue of  $M_x^{red}$ ).
- An orbit is *non-degenerate* if 1 does not appear among its Floquet multipliers.
- An orbit is *stable* if all its Floquet multipliers are semi-simple and lie in the unit circle.

We will only consider the cases  $n = 2$  (planar problems) and  $n = 3$  (spatial problems).

**Symmetries.** An *anti-symplectic involution* is a map  $\rho : M \rightarrow M$  satisfying  $\rho^2 = id$  and  $\rho^*\omega = -\omega$ . Its *fixed-point locus* is  $fix(\rho) = \{x : \rho(x) = x\}$ . An anti-symplectic involution  $\rho$  is a *symmetry* of the system if  $H \circ \rho = H$ . A periodic orbit  $x$  is *symmetric* if  $\rho(x(-t)) = x(t)$  for all  $t$ . The *symmetric points* of the symmetric orbit  $x$  are the two intersection points of  $x$  with  $fix(\rho)$ . The monodromy matrix of a symmetric orbit at a symmetric point is a *Wonenburger* matrix:

$$M = M_{A,B,C} = \begin{pmatrix} A & B \\ C & A^T \end{pmatrix} \in Sp(2n), \quad (1)$$

where

$$B = B^T, \quad C = C^T, \quad AB = BA^T, \quad A^T C = CA, \quad A^2 - BC = id,$$

equations which ensure that  $M$  is symplectic. The eigenvalues of  $M$  are determined by those of the first block  $A$ :<sup>1</sup>

- If  $\lambda$  is an eigenvalue of  $M$  then its stability index  $a(\lambda) = \frac{1}{2}(\lambda + 1/\lambda)$  is an eigenvalue of  $A$ .
- If  $a$  is an eigenvalue of  $A$  then  $\lambda(a) = a + \sqrt{a^2 - 1}$  is an eigenvalue of  $M$ .

### B-signs

Assume  $n = 2, 3$ . Let  $x$  be a symmetric orbit with monodromy  $M_{A,B,C}$  at a symmetric point. Assume  $a$  is a real, simple and nontrivial eigenvalue of  $A$  (i.e.  $\lambda(a)$  elliptic or hyperbolic). Let  $v$  be an eigenvector of  $A^T$  with eigenvalue  $a$ , i.e.  $A^T v = a \cdot v$ . The *B-sign* of  $\lambda(a)$  is

$$\epsilon(\lambda(a)) = \text{sign}(v^T B v) = \pm.$$

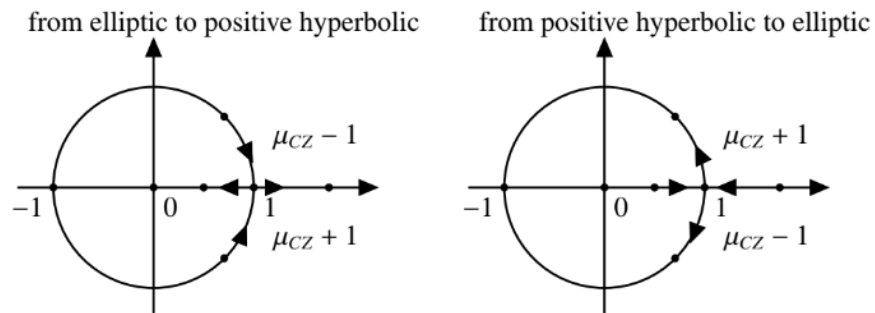


**Figure 1.**  $\mu_{CZ}$  jumps by  $\pm 1$  when crossing 1, according to direction of bifurcation, as shown. If it stays elliptic, the jump is by  $\pm 2$ . This is determined by the  $B$ -sign.

One easily sees that this is independent of  $v$ , and the basis chosen to write down the monodromy matrix. Note that if  $n = 2$ , we have two  $B$ -signs  $\epsilon_1, \epsilon_2$ , one for each symmetric point; and if  $n = 3$ , we have two *pairs* of  $B$ -signs  $(\epsilon_1^1, \epsilon_2^1), (\epsilon_1^2, \epsilon_2^2)$ , one for each symmetric point and each eigenvalue.

The second and fourth authors have recently shown that a planar symmetric orbit is negative hyperbolic iff the  $B$ -signs of its two symmetric points differ.<sup>10</sup> One can define the  $C$ -signs similarly, obtained by replacing the  $B$ -block, with the  $C$ -block of  $M$ , and  $A^T$ , by  $A$ .

### Conley–Zehnder index

The CZ-index is part of the index theory of the symplectic group. It assigns a winding number to non-degenerate orbits. In practical terms, it helps understand which families of orbits connect to which (CZ-index stays constant if no bifurcation occurs, and jumps under bifurcation as shown in Figure 1). It may be defined as follows.

**Planar case.** Let  $n = 2$ ,  $x$  planar orbit with (reduced) monodromy  $M_x^{red}$ , and  $x^k$  its  $k$ -fold cover.

- **Elliptic case:**  $M_x^{red}$  is conjugated to a rotation,

$$M_x^{red} \sim \begin{pmatrix} \cos \varphi & -\sin \varphi \\ \sin \varphi & \cos \varphi \end{pmatrix}, \quad (2)$$

with Floquet multipliers  $e^{\pm 2\pi i \varphi}$ . Then

$$\mu_{CZ}(x^k) = 1 + 2 \cdot \lfloor k \cdot \varphi / 2\pi \rfloor$$

In particular, it is odd, and jumps by  $\pm 2$  if the eigenvalue 1 is crossed in a family. Recall from (1) that for symmetric periodic orbits we have  $M_x^{red} = \begin{pmatrix} a & b \\ c & a \end{pmatrix}$ . Moreover, in view of (2) if  $b < 0$  then the rotation is determined by  $\varphi$  and if  $b > 0$  then the rotation is determined by  $-\varphi$ ; this determines the CZ-index jump, see Figure 1.

- **Hyperbolic case:**  $M_x^{red}$  is diagonal up to conjugation,

$$M_x^{red} \sim \begin{pmatrix} \lambda & 0 \\ 0 & 1/\lambda \end{pmatrix},$$

with Floquet multipliers  $\lambda, 1/\lambda$ . Then

$$\mu_{CZ}(x^k) = k \cdot n,$$

where  $D\phi_t^H$  rotates the eigenspaces by angle  $\frac{\pi nt}{T}$ , with  $n$  even/odd if  $x$  positive/negative hyperbolic. Notice that for symmetric periodic orbits the signatures of  $b$  and  $c$  are equal.

**Spatial case.** Let  $n = 3$ . Assume that the reflection along the  $xy$ -plane gives rise to a symplectic symmetry of  $H$  (e.g., the 3BP). If  $x \subset \mathbb{R}^2$  is a planar orbit, then we have a symplectic splitting into planar and spatial blocks

$$M_x^{red} \sim \begin{pmatrix} M_p^{red} & 0 \\ 0 & M_s \end{pmatrix} \in Sp(4), \quad M_p^{red}, M_s \in Sp(2).$$

Then

$$\mu_{CZ}(x) = \mu_{CZ}^p(x) + \mu_{CZ}^s(x),$$

where each summand corresponds to  $M_p^{red}$  and  $M_s$  respectively. We have that

- Planar to planar bifurcations correspond to jumps in  $\mu_{CZ}^p$ .
- Planar to spatial bifurcations correspond to jumps of  $\mu_{CZ}^s$ .

While the CZ-index is defined in general, all our bifurcations will involve planar-to-spatial bifurcations at planar orbits and the above symmetry, so these definitions will suffice. In what follows, the computations of CZ-indices of families will not rely directly on the definition, but rather on knowing them analytically for special families (e.g., in the Kepler problem), and then determining the jumps at bifurcations arising after deformation, for which the  $B$ -signs are necessary, as explained above.

### Floer numerical invariants

Recall that bifurcations occurs when studying families  $t \mapsto x_t$  of periodic orbits, as a mechanism by which at some parameter time  $t = t_0$  the orbit  $x_{t_0}$  becomes degenerate, and several new families may bifurcate out of it; see Figure 2. The Floer numbers are meant to give a simple test to keep track of all new families. We will first need the following technical definition: a periodic orbit  $x$  is *good* if

$$\mu_{CZ}(x^k) = \mu_{CZ}(x) \bmod 2$$

for all  $k \geq 1$ . Otherwise, it is *bad*. In fact, a planar orbit is bad iff it is an even cover of a negative hyperbolic orbit. And a spatial orbit is bad iff it is an even cover of either an elliptic-negative hyperbolic or a positive-negative hyperbolic orbit. Note that a good planar orbit can be bad if viewed in the spatial problem.

Given a bifurcation at  $x$ , the *SFT-Euler characteristic* (or the *Floer number*) of  $x$  is

$$\chi(x) = \sum_i (-1)^{CZ_i^{bef}} = \sum_j (-1)^{CZ_j^{aft}}.$$

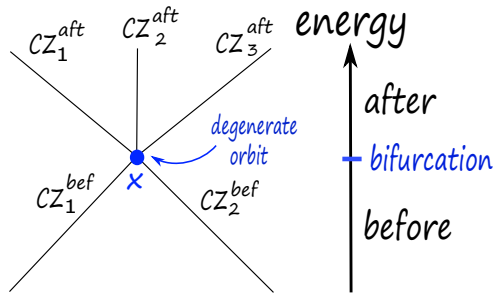


**Figure 2.** A sketch of a bifurcation at a degenerate orbit, with the before/after orbits determined by the deformation parameter (the energy), each branch with its own CZ-index. The Floer number is a signed count of orbits which stays invariant.

The sum on the LHS is over **good** orbits *before* bifurcation, and RHS is over **good** orbits *after* bifurcation. As these numbers only involve the parity of the CZ-index, one has simple formulas which bypass the computation of this index, as they only involve the Floquet multipliers:

- **Planar case.**  $\chi(x) = \#\{\text{good } \mathcal{H}^+\} - \#\{\mathcal{E}, \mathcal{H}^-\}$ .
- **Spatial case.**  $\chi(x) = \#\{\mathcal{H}^{--}, \mathcal{E}\mathcal{H}^-, \mathcal{E}^2, \text{good } \mathcal{H}^{++}, \mathcal{N}\} - \#\{\mathcal{H}^{-+}, \text{good } \mathcal{E}\mathcal{H}^+\}$ .

Here,  $\mathcal{E}$  denotes *elliptic*,  $\mathcal{H}^\pm$  denotes *positive/negative hyperbolic*, and  $\mathcal{N}$  denotes *nonreal* quadruples  $\lambda, 1/\lambda, \bar{\lambda}, 1/\bar{\lambda}$ . The above simply tells us which type of orbit comes with a plus or a minus sign (the formula should be interpreted as either before or after).

**Invariance.** The fact that the sums agree before and after *–invariance–* follows from deep results from *Floer theory* in symplectic geometry. We will accept this as a fact, and use it as follows:

The Floer number can be used as a **test**: if the sums do *not* agree, we know the algorithm missed an orbit.

The invariant above works for arbitrary periodic orbits. There is a similar Floer invariant for *symmetric* orbits.<sup>3</sup>

## Global topological methods

These methods encode: bifurcations; stability; eigenvalue configurations; obstructions to existence of regular families; and *B*-signs, in a visual and resource-efficient way. The main tool is the *GIT sequence*,<sup>1</sup> a refinement of the Broucke stability diagram via implementing the *B*-signs. This is a sequence of three branched spaces (or *layers*), together with two maps between them, which collapse certain branches together. Each branch is labelled by the *B*-signs. A symmetric orbit gives a point in the top layer, and an arbitrary orbit, in the middle layer. The base layer is  $\mathbb{R}^n$  (the space of coefficients of the characteristic polynomial of the first block of  $M_{A,B,C}$ ). Then a family of orbits gives a path in these spaces, so that their topology encodes valuable information. The details are as follows.

**GIT sequence: 2D.** Let  $n = 2$ ,  $\lambda$  eigenvalue of  $M^{red} \in Sp(2)$ , with stability index  $a(\lambda) = \frac{1}{2}(\lambda + 1/\lambda)$ . Then  $\lambda = \pm 1$  iff  $a(\lambda) = \pm 1$ ;  $\lambda$  positive hyperbolic iff  $a(\lambda) > 1$ ;  $\lambda$  negative hyperbolic iff  $a(\lambda) < -1$ ; and  $\lambda$  elliptic (stable) iff  $-1 < a(\lambda) < 1$ . The Broucke stability diagram is

then simply the real line, split into three components; see Figure 3. If two orbits lie in different components of the diagram, then one should expect bifurcations in any family joining them, as the topology of the diagram implies that any path between them has to cross the  $\pm 1$  eigenvalues.

One can think that the stability index “collapses” the two elliptic branches in the middle layer of Figure 3 together. These two branches are distinguished by the  $B$ -signs, coinciding with the Krein signs.<sup>5,6</sup> There is an extra top layer for symmetric orbits, where now each hyperbolic branch separates into two, and there is a collapsing map from the top to middle layer. Note that to go from one branch to the other, the topology of the layer implies that the eigenvalue 1 needs to be crossed. This means that one should expect bifurcations in any (symmetric) family joining them, *even if* they project to the same component of the Broucke diagram. To sum up:

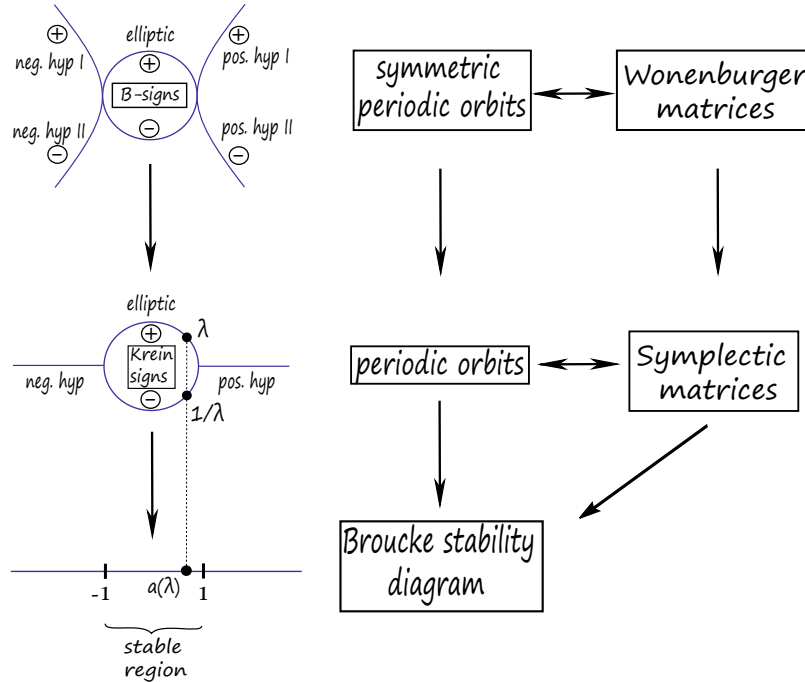


**Figure 3. The 2D GIT sequence. One obtains more refined information for symmetric orbits.**

- $B$ -signs “separate” hyperbolic branches, for symmetric orbits.
- If two points lie in different components of the Broucke diagram, one should expect bifurcation in any path joining them.
- If two points lie in the same component of the Broucke diagram, but if  $B$ -signs differ, one should *also* expect bifurcation in any path joining them.

**GIT sequence: 3D.** Let  $n = 3$ . Given  $M^{red} = M_{A,B,C} \in Sp(4)$ , its *stability point* is  $p = (\text{tr}(A), \det(A)) \in \mathbb{R}^2$ . The plane splits into regions corresponding to the eigenvalue configuration of  $M^{red}$ , as in Figure 4. The GIT sequence<sup>1</sup> adds two layers to this diagram, as shown in Figure 5. The top layer has two extra branches than the middle one, for each hyperbolic eigenvalue.

**Bifurcations in the Broucke diagram.** An orbit family  $t \mapsto x_t$  gives a path  $t \mapsto p_t \in \mathbb{R}^2$  of

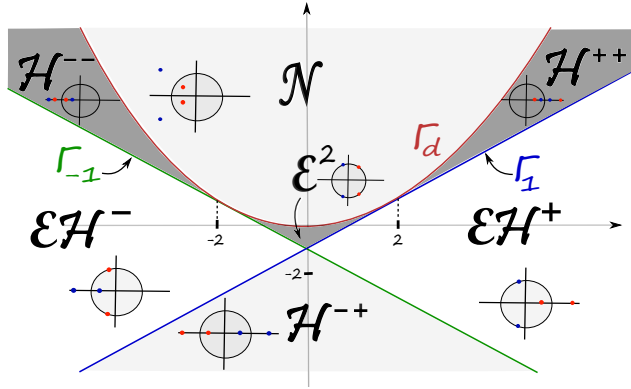


**Figure 4.** The 3D Broucke stability diagram. Here,  $\Gamma_{\pm 1}$  corresponds to eigenvalue  $\pm 1$ ,  $\Gamma_d$  to double eigenvalue,  $\mathcal{E}^2$  to doubly elliptic (stable region), and so on.<sup>1</sup>

stability points. The family bifurcates if  $p_t$  crosses  $\Gamma_1$ . More generally, let  $\Gamma_\varphi^e$  be the line with slope  $\cos(2\pi\varphi) \in [-1, 1]$  tangent to  $\Gamma_d = \{y = x^2/4\}$ , corresponding to matrices with eigenvalue  $e^{2\pi i\varphi}$ ; and  $\Gamma_\lambda^h$  the tangent line with slope  $a(\lambda) \in \mathbb{R} \setminus [-1, 1]$ , corresponding to matrices with eigenvalue  $\lambda$ .

A  $k$ -fold bifurcation happens when crossing  $\Gamma_{l/k}^e$  for some  $l$ .

That is, higher order bifurcations are encoded by a pencil of lines tangent to a parabola, as in Figure 6.

**Example: symmetric period doubling bifurcation.** We finish this section with an example where our invariants give new information. Consider a symmetric orbit  $x$  going from elliptic to negative hyperbolic. A priori there could be two bifurcations, one for each symmetric point (B or C in Figure 7). However, invariance of  $\chi(x^2)$  implies only *one* can happen (note  $x^2$  is bad). And where the bifurcation happens is determined by the  $B$ -sign, occurring at the symmetric point in which the  $B$ -sign does *not* jump; or alternatively, where the  $C$ -sign jumps.

### Circular restricted three-body problem

The Circular Restricted Three-Body Problem (CRTBP) shown in Figure 8 describes the motion of an infinitesimal mass with two primaries under mutual gravitational attraction. A dimensionless rotating coordinate system  $(X^R - Y^R - Z^R)$  is defined at the barycenter of the two primaries with respect to the inertial frame  $(X^I - Y^I - Z^I)$ , rotating about  $Z^I$  with true anomaly  $\nu$ . The  $X$ -axis of the rotating coordinate system is aligned with the vector from the larger primary body ( $m_1$ ) to the second primary body ( $m_2$ ). The  $Z$ -axis is perpendicular to the primaries' orbital plane, and the  $Y$ -axis completes the right-handed coordinate system. The position vector  $\mathbf{r}$  points from the barycenter to the spacecraft in the rotating frame. The non-dimensional mass of the second primary is defined as

$$\mu = \frac{m_2}{m_1 + m_2} = m_2,$$

and then the larger body's mass is

$$1 - \mu = \frac{m_1}{m_1 + m_2} = m_1.$$



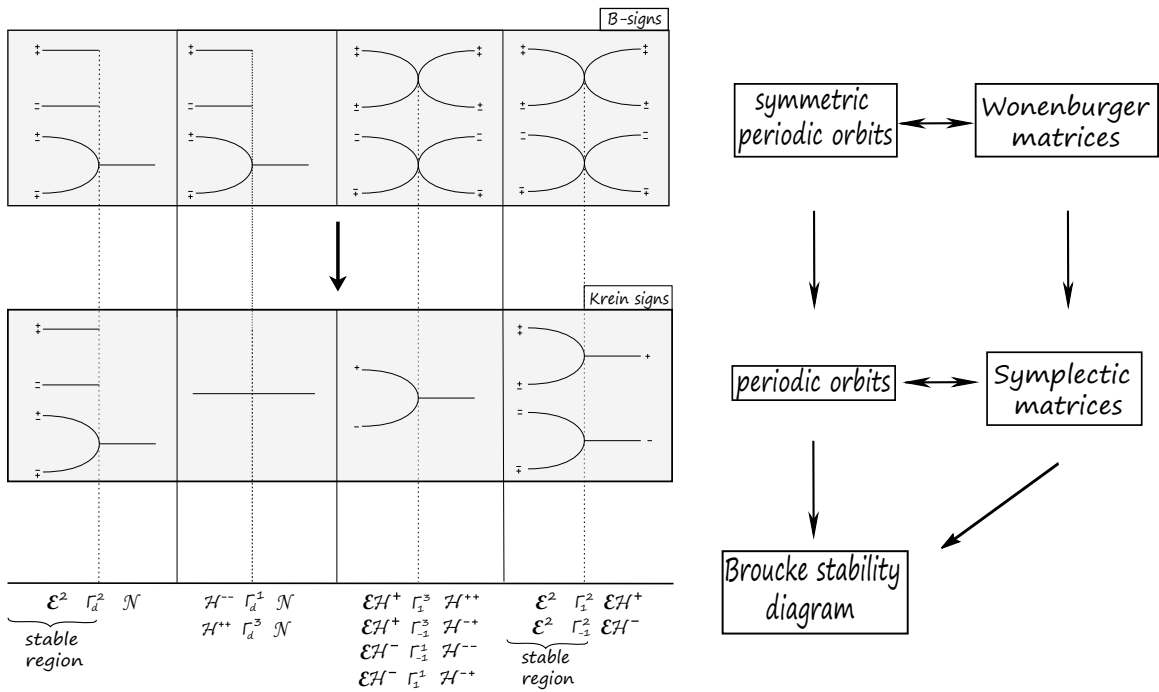


Figure 5. The branches (represented as lines) are two-dimensional, and come together at the 1-dimensional “branching locus” (represented as points), where we cross from one region to another of the Broucke diagram.

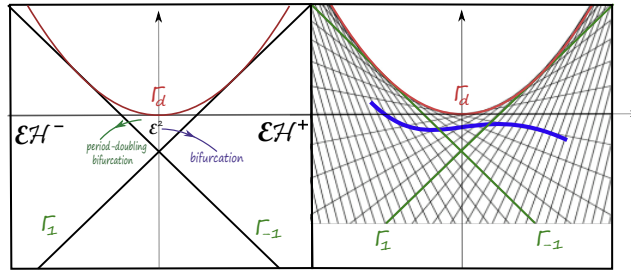


Figure 6. Bifurcations are encoded by a pencil of lines.

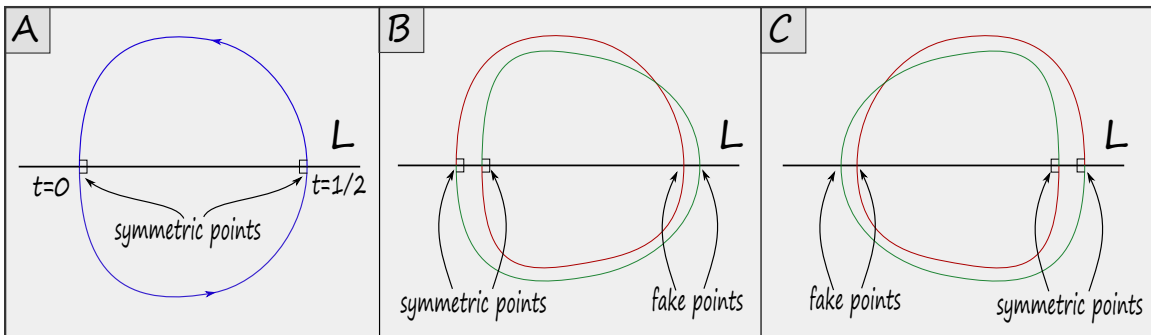
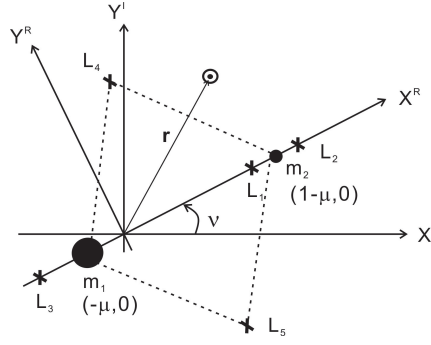


Figure 7. Symmetric period doubling bifurcation. The *fake* symmetric points, while close to intersection points, do *not* intersect the fixed-point loci.



**Figure 8.** A schematic CRTBP configuration showing  $x_1 = m_1$ ,  $x_2 = m_2$ , and two of the libration points in a non-dimensional rotating coordinate system  $X^R - Y^R$ ,  $Z^R(Z^I)$  are in the out-of-plane direction.

Define the unit of time so that the mean motion of the primary orbit is 1. Then the equations of motion for the infinitesimal mass is written as

$$\begin{aligned}\ddot{x} &= 2\dot{y} + x - (1 - \mu) \frac{x + \mu}{r_1^3} - \mu \frac{x - 1 + \mu}{r_2^3} \\ \ddot{y} &= -2\dot{x} + y - (1 - \mu) \frac{y}{r_1^3} - \mu \frac{y}{r_2^3} \\ \ddot{z} &= -(1 - \mu) \frac{z}{r_1^3} - \mu \frac{z}{r_2^3}\end{aligned}$$

where  $r_1^2 = (x + \mu)^2 + y^2 + z^2$ ,  $r_2^2 = (x - 1 + \mu)^2 + y^2 + z^2$ . No closed form general solution is possible for the model.

The Hamiltonian describing the CRTBP is given by

$$\begin{aligned}H &: (\mathbb{R}^3 \setminus \{M, P\}) \times \mathbb{R}^3 \rightarrow \mathbb{R}, \\ H(q, p) &= \frac{1}{2} \|p\|^2 - \frac{\mu}{\|q - M\|} - \frac{1 - \mu}{\|q - P\|} + p_1 q_2 - p_2 q_1,\end{aligned}$$

where  $q = (q_1, q_2, q_3)$  is the position of a satellite,  $p = (p_1, p_2, p_3)$  is its momentum, the mass of the secondary body  $m_2$  is fixed at  $M = (1 - \mu, 0, 0)$ , and the mass of the primary body  $m_1$  is fixed at  $P = (-\mu, 0, 0)$ . The Jacobi constant  $c$  is then defined by the convention  $\Gamma := H \equiv -c/2$ . The Hamiltonian  $H$  is invariant under the anti-symplectic involutions

$$\begin{aligned}\rho &: (q_1, q_2, q_3, p_1, p_2, p_3) \mapsto (q_1, -q_2, -q_3, -p_1, p_2, p_3), \\ \tilde{\rho} &: (q_1, q_2, q_3, p_1, p_2, p_3) \mapsto (q_1, -q_2, q_3, -p_1, p_2, -p_3),\end{aligned}$$

with corresponding fixed-point loci given by

$$\begin{aligned}L &= \text{Fix}(\rho) = \{q_2 = q_3 = p_1 = 0\}, \\ \tilde{L} &= \text{Fix}(\tilde{\rho}) = \{q_2 = p_1 = p_3 = 0\}.\end{aligned}$$

These correspond respectively to  $\pi$ -rotation around the  $x$ -axis, and reflection along the  $xz$ -plane. Their composition  $\sigma = \rho \circ \tilde{\rho}$  is a *symplectic* symmetry corresponding to reflection along the  $xy$ -plane.

For instance, the *Jupiter-Europa system* then corresponds to a CRTBP with mass ratio  $\mu = 2.5266448850435e^{-05}$ .

## Hill's lunar problem

Hill's lunar problem is a limit case of the restricted three-body problem where the massless body is assumed very close to the small primary. This problem can therefore be viewed as an approximation to the Jupiter-Europa system, when one lets the mass of Europa go to zero. The Hamiltonian describing the system is

$$E : (\mathbb{R}^3 \setminus \{0\}) \times \mathbb{R}^3 \rightarrow \mathbb{R},$$

$$E(q, p) = \frac{1}{2} \|p\|^2 - \frac{1}{\|q\|} + p_1 q_2 - p_2 q_1 - q_1^2 + \frac{1}{2} q_2^2 + \frac{1}{2} q_3^2.$$

The linear symmetries of this problem have been completely characterized.<sup>11</sup> While the planar restricted three-body problem is invariant under reflection at the  $x$ -axis, the planar Hill lunar problem is additionally invariant under reflection at the  $y$ -axis. For the spatial lunar problem, there are more symmetries:  $\rho, \tilde{\rho}$  (which extend the reflection at the  $x$ -axis), and two additional symmetries  $\kappa, \tilde{\kappa}$  ( $\pi$ -rotation along the  $y$ -axis, and reflection along the  $yz$ -plane; both extend the reflection along the  $y$ -axis). Their composition is also  $\sigma = \kappa \circ \tilde{\kappa}$ .

## NUMERICAL WORK

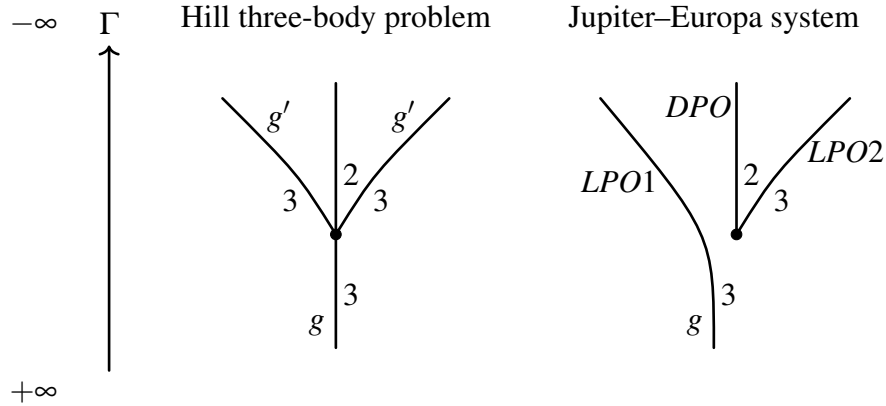
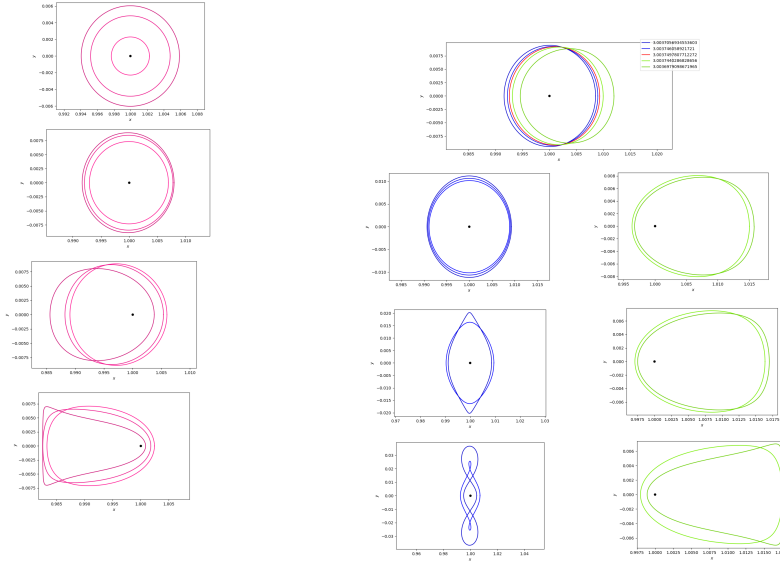


Figure 9. Bifurcation graphs for the planar direct/prograde orbits with CZ-index.

### Result I. Planar direct / prograde orbits

Hénon<sup>12</sup> describes a family  $g$  of planar direct periodic orbits which are invariant with respect to both reflections at the  $x$  and  $y$ -axis. This family undergoes a non-generic pitchfork bifurcation, going from elliptic to positive hyperbolic, and where two new families of elliptic orbits, called  $g'$ , appear; see Figure 9. These new families are still invariant under reflection at the  $x$ -axis, but not under reflection at the  $y$ -axis. Reflection at the  $y$ -axis maps one branch of the  $g'$ -family to the other branch. Figure 9 shows the bifurcation graph which is constructed as follows: Each vertex denotes a degenerate orbit at which bifurcation happens and each edge represents a family of orbits with varying energy, labeled by the corresponding CZ-index. From this data, it is easy to determine the associated Floer number. For instance in Figure 9 on the left, the Floer number is  $(-1)^3 = -1$  before bifurcation, and  $(-1)^2 + 2(-1)^3 = -1$  after bifurcation; they coincide, as they should.

By deforming the mass parameter, we may go from Hill's lunar problem to the Jupiter-Europa system; see Figure 9. The pitchfork bifurcation deforms to a *generic* situation, where one of the



**Figure 10.** Left: the  $g$ -LPO1 branch, where the energy increases from top to bottom. Right: the DPO-LPO2 branch, split into the DPO sub-branch (left, where orbits are planar positive hyperbolic) and of the LPO2 sub-branch (right, where orbits are planar elliptic). The red orbit is the degenerate orbit, undergoing birth-death bifurcation. The Jacobi constant  $\Gamma = -2c$  is shown on the upper right side, reaching a maxima at the red orbit.

$g'$  branches glues to the before-bifurcation part of the  $g$  branch, the result of which we call the  $g$ -LPO1 branch, and where the other  $g'$  branch glues to the after-bifurcation part of the  $g$  branch, which we call the  $DPO$ -LPO2 branch (undergoing birth-death bifurcation). The  $DPO$ -orbits are planar positive hyperbolic and the  $LPO2$ -orbits are planar elliptic. As the symmetry with respect to the  $y$ -axis is lost, the new orbits will be *approximately* symmetric with respect to the  $y$ -axis, but not exactly symmetric; similarly, the  $y$ -symmetric relation between the  $g'$  branches persists only approximately for the corresponding deformed orbits. These families are plotted in Figure 10, where this behavior is manifest. The data for each new branch is given in Tables 1, 2 and 3 in the Appendix. Via this bifurcation analysis, one may predict the existence of the  $DPO$ -LPO2 branch, which a priori is not straightforward to find. While these families are already known and appear e.g., in page 12 of Reference 13, this suggests a general mechanism which we will exploit, cf. Figure 13, and Figure 14. Note that Reference 13 provides an online data base for *planar* and *x-axis symmetric* periodic orbits, and we match their notation for orbits ( $DPO$ ,  $LPO$ , etc.). The novelty of this article is to focus on *spatial* bifurcations of these planar orbits, employing our novel methods.

## Result II. One example of bifurcation graphs for planar-to-spatial bifurcation with the same topology

The spatial CZ-index of the simple closed  $DPO$ -orbit at around  $\Gamma = 3.00109352$  jumps by  $+1$ , see Table 2 in the Appendix. Therefore it generates a planar-to-spatial bifurcation, see the plot in Figure 11. As in Hill's problem, this new family of spatial orbits appears twice by using the reflection at the  $xy$ -plane. Surprisingly, compared to Figure 9, because the symmetry is preserved, the bifurcation graph has the same topology after deformation and is still non-generic, see the graph in Figure 12.

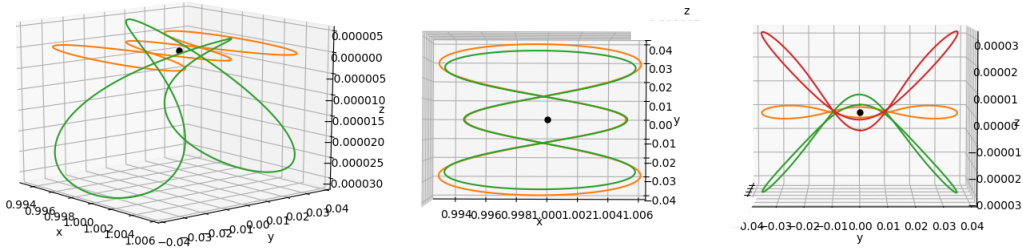


**Figure 11. Jupiter-Europa: A planar-to-spatial bifurcation of a simple closed planar DPO orbit, from the side, from above and with its symmetric family by using the reflection at the  $xy$ -plane.**

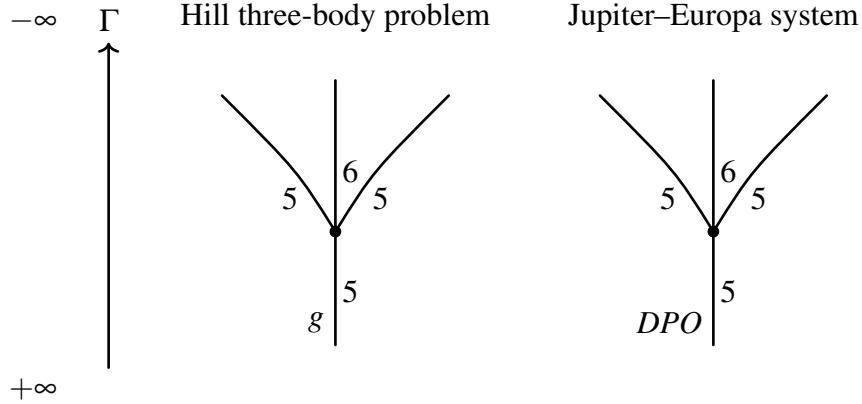


**Figure 12. Left: The bifurcation graph between simple closed  $g$ -orbit and the new families of spatial orbits generated by the spatial index jump in Hill's system. Right: In the Jupiter-Europa system. The horizontal symmetry corresponds to the reflection at the  $xy$ -plane.**

### Result III. Bifurcation graphs between third covers of prograde and fifth cover of retrograde orbits

A bifurcation graph relating third covers of  $g$ ,  $g'$ , and fifth covers of planar retrograde orbits, known as family  $f$ , was obtained by the first author;<sup>4</sup> see Figure 13. The third covers of LPO2 and fifth covers of DRO were found using Cell-Mapping.<sup>14</sup> Taking Fig. 13 as a starting point, we compare it to the Jupiter-Europa system. The result is plotted in Figure 14.

Let us focus on the two vertices on the right of Figure 13 which are not of birth-death type. After deformation, the (red) family starting at  $g'^3$  on the right of CZ-index 15 glues to the (blue) family of the same index ending in  $f^5$ , resolving the vertex at which they meet; note that similarly as in Result I,  $f$  is replaced with DRO, and  $g'$ , with LPO2. The two other families meeting at the same vertex coming from  $g'^3$  and  $g^3$  now glue to a family undergoing birth-death, where now  $g'$  is replaced by  $g$ -LPO1, and  $g$ , with DPO. A similar phenomenon happens at the other vertex, where the (pink) family starting at  $g'^3$  with CZ-index 14 on the right glues to the (green) family of the same index, and the other two families now undergo birth-death.

Another notable feature is the (red) family between  $LPO2^3$  and  $DRO^5$  of CZ-index 15, a *spatial* family connecting two *planar* orbits, one retrograde ( $DRO^5$ ), and the other, prograde ( $LPO2^3$ ).

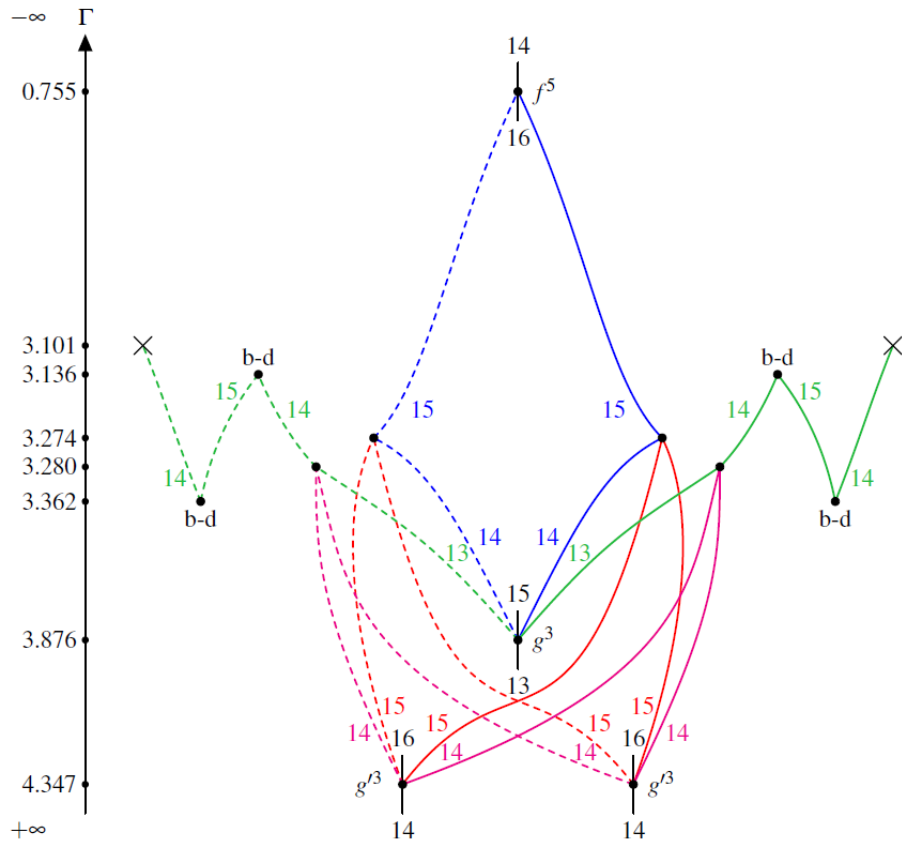


**Figure 13.** Bifurcation graph for Hill's lunar problem by the first author,<sup>4</sup> between the 3rd cover of  $g$ , the 3rd cover of  $g'$  and the 5th cover of  $f$ , based on work of Kalantonis.<sup>15</sup> A cross means collision, and b-d means birth-death bifurcation. The horizontal symmetry in the diagram, relating full and dashed edges, means that the corresponding families are related by a symmetry. For instance, the non-dashed red 15 on the right is related by the dashed red 15 on the right by reflection along the  $xy$ -plane. The other red 15 families on the left are obtained by applying the extra two spatial symmetries  $\tilde{K}, \tilde{K}'$ . Similarly for the pink 14 families. The blue and green families are doubly symmetric; one of the symmetries breaks at bifurcation, where the red and pink families appear.

## CONCLUSION

We presented a toolkit extracted from the general methods of symplectic geometry/topology, aimed at studying periodic orbits of general Hamiltonian systems, together with their bifurcations in families, eigenvalue configurations, and stability, in a visual, and resource-efficient way. In the presence of symmetry, the information attached to orbits, and the methods involved, may be significantly refined. We illustrated these methods on numerical examples, for a system of current interest which is modelled by a restricted three-body problem (Jupiter-Europa). We have studied families of planar to spatial bifurcations for this system, via bifurcation analysis and deformation from the lunar problem. The numerical findings are in agreement with the theoretical predictions, and the bifurcation graphs are completely novel.

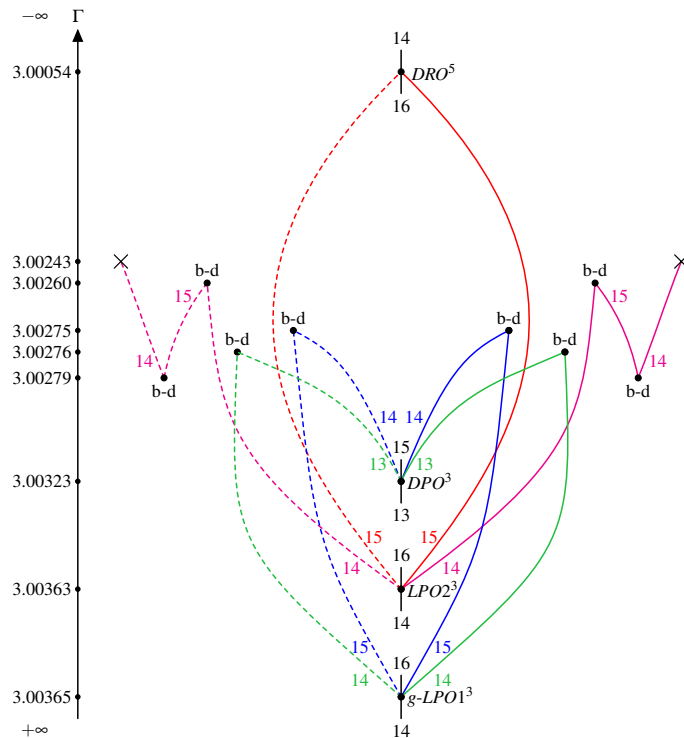


**Figure 14.** Bifurcation graph for the Jupiter–Europa system, between the 3rd cover of  $g-LPO1$ , the third cover of  $DPO$ , the third cover of  $LPO2$ , and the 5th cover of  $DRO$ . The data for the pink family is collected in Table 5, for the red one in Table 6, for the blue one in Table 7 and for the green in Table 8. Some orbits of the blue and green family are plotted in Figure 15. The horizontal symmetry is reflection along the  $xy$ -plane. Note that non-dashed red 15 and non-dashed blue 15 are no longer related by a symmetry.

## ACKNOWLEDGMENT

A. Moreno is supported by the NSF under Grant No. DMS-1926686, by the Sonderforschungsbereich TRR 191 Symplectic Structures in Geometry, Algebra and Dynamics, funded by the DFG (Projektnummer 281071066 – TRR 191), and by the DFG under Germany’s Excellence Strategy EXC 2181/1 - 390900948 (the Heidelberg STRUCTURES Excellence Cluster).

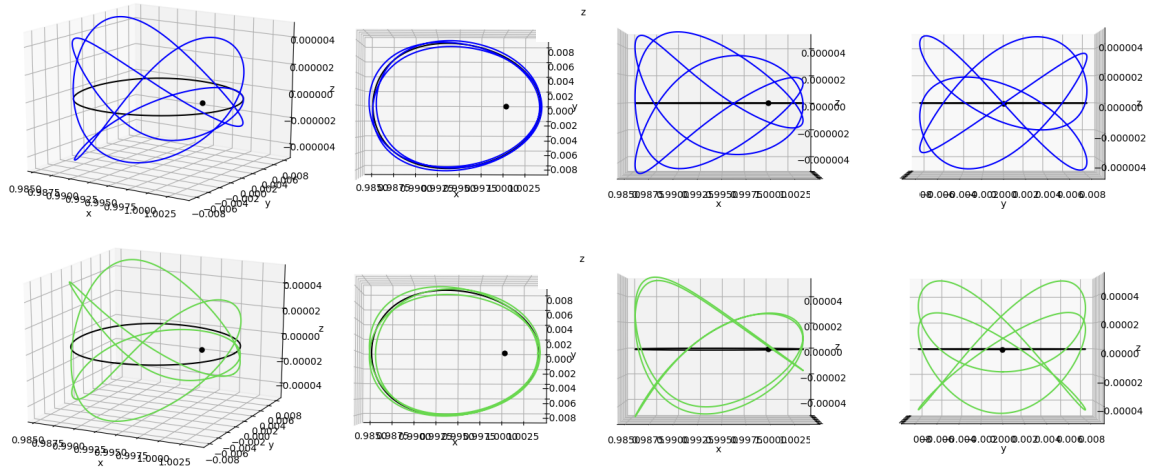


**Figure 15. Jupiter-Europa: Two families of spatial orbits branching out from the  $g$ - $LPO13^3$  orbit; above: these orbits are symmetric w.r.t. the  $x$ -axis and their data is collected in Table 7. This is the (blue) family of CZ-index 15 in Figure 14; below: these orbits are symmetric w.r.t. the  $xz$ -plane and their data is collected in Table 8. This is the (green) family of CZ-index 14 in Figure 14. Each family has a symmetric family by using the reflection at the ecliptic.**



**APPENDIX: TABLES**

**Table 1. Data for  $g$ -LPO1 branch.**

$\Gamma$	$x(0)$	$\dot{y}(0)$	$T$	(C/B)-sign & Floquet multipliers	$\mu_{CZ}^p / \mu_{CZ}^s / \mu_{CZ}$
3.01142113	1.0226290	0.10284894	0.13999	(+/-) $\varphi_p = 0.137$ , (+/-) $\varphi_s = 0.142$	3 / 3 / 6
3.00383366	1.00797270	0.05073828	1.17402	(+/-) $\varphi_p = 0.332$ , (+/-) $\varphi_s = 1.290$	3 / 3 / 6
3.00372747	1.00538715	0.07480305	1.33771	(+/-) $\varphi_p = 0.556$ , (+/-) $\varphi_s = 1.572$	3 / 3 / 6
3.00365597	1.00378076	0.09779235	1.59835	(+/-) $\varphi_p = 1.068$ , (+/-) $\varphi_s = 2.089$	3 / 3 / 6
3.00360358	1.00244635	0.12945606	2.08332	(+/-) $\varphi_p = 1.845$ , (+/-) $\varphi_s = 3.136$	3 / 3 / 6
3.00360326	1.00243628	0.12977936	2.08832	(+/-) $\varphi_p = 1.858$ , (+/+) $\lambda_s = -1.03$	3 / 3 / 6
3.00360049	1.00234732	0.13271728	2.13332	(+/-) $\varphi_p = 1.987$ , (+/+) $\lambda_s = -1.05$	3 / 3 / 6
3.00359960	1.00231829	0.13370950	2.14831	(+/-) $\varphi_p = 2.037$ , (-/+) $\varphi_s = 3.166$	3 / 3 / 6
3.00358255	1.00180287	0.15481646	2.43323	(+/+) $\lambda_p = -4.39$ , (-/+) $\varphi_s = 3.796$	3 / 3 / 6
3.00343430	1.00043030	0.32769866	3.13136	(+/+) $\lambda_p = -129$ , (-/+) $\varphi_s = 5.223$	3 / 3 / 6

**Table 2. Data for DPO branch.**

$\Gamma$	$x(0)$	$\dot{y}(0)$	$T$	(C/B)-sign & Floquet multipliers	$\mu_{CZ}^p / \mu_{CZ}^s / \mu_{CZ}$
3.00374605	1.00900895	0.04460670	1.25362	(-/-) $\lambda_p = 1.29$ , (+/-) $\varphi_s = 1.385$	2 / 3 / 5
3.00358658	1.00884026	0.04739922	1.41448	(-/-) $\lambda_p = 2.23$ , (+/-) $\varphi_s = 1.565$	2 / 3 / 5
3.00356924	1.00889026	0.04727261	1.43426	(-/-) $\lambda_p = 2.36$ , (+/-) $\varphi_s = 1.589$	2 / 3 / 5
3.00340053	1.00928559	0.04673515	1.64653	(-/-) $\lambda_p = 4.29$ , (+/-) $\varphi_s = 1.829$	2 / 3 / 5
3.00323697	1.00958786	0.04684116	1.88433	(-/-) $\lambda_p = 8.52$ , (+/-) $\varphi_s = 2.094$	2 / 3 / 5
3.00257321	1.00913170	0.05562606	2.88768	(-/-) $\lambda_p = 136$ , (+/-) $\varphi_s = 3.092$	2 / 3 / 5
3.00237147	1.00863170	0.05990199	3.16288	(-/-) $\lambda_p = 246$ , (-/+) $\varphi_s = 3.334$	2 / 3 / 5
3.00109352	1.00470170	0.09778837	5.12979	(-/-) $\lambda_p = 2485$ , (-/+) $\varphi_s = 6.161$	2 / 3 / 5
3.00109192	1.00469670	0.09785369	5.13303	(-/-) $\lambda_p = 2570$ , (+/+) $\lambda_s = 1.027$	2 / 4 / 6
3.00107109	1.00463170	0.09871030	5.17546	(-/-) $\lambda_p = 3062$ , (+/+) $\lambda_s = 1.540$	2 / 4 / 6

**Table 3. Data for LPO2 branch.**

$\Gamma$	$x(0)$	$\dot{y}(0)$	$T$	(C/B)-sign & Floquet multipliers	$\mu_{CZ}^p / \mu_{CZ}^s / \mu_{CZ}$
3.00374885	1.00955895	0.04118756	1.25694	(+/-) $\varphi_p = 0.190$ , (+/-) $\varphi_s = 1.397$	3 / 3 / 6
3.00371150	1.01150895	0.03105844	1.34143	(+/-) $\varphi_p = 0.538$ , (+/-) $\varphi_s = 1.555$	3 / 3 / 6
3.00369790	1.01200895	0.02882949	1.37591	(+/-) $\varphi_p = 0.625$ , (+/-) $\varphi_s = 1.620$	3 / 3 / 6
3.00363027	1.01440084	0.01977091	1.62295	(+/-) $\varphi_p = 1.101$ , (+/-) $\varphi_s = 2.094$	3 / 3 / 6
3.00357414	1.016776	0.0130372	2.1215	(+/-) $\varphi_p = 1.878$ , (+/-) $\varphi_s = 3.131$	3 / 3 / 6
3.00357388	1.016787	0.013014	2.12519	(+/-) $\varphi_p = 1.885$ , (-/-) $\lambda_s = -1.02$	3 / 3 / 6
3.00356878	1.01701395	0.01253366	2.20708	(+/-) $\varphi_p = 2.120$ , (-/+ ) $\varphi_s = 3.225$	3 / 3 / 6
3.00353952	1.01771395	0.01187914	2.65553	(+/+) $\lambda_p = -9.64$ , (-/+ ) $\varphi_s = 4.144$	3 / 3 / 6
3.00349789	1.01765259	0.01364657	2.95454	(+/+) $\lambda_p = -36.3$ , (-/+ ) $\varphi_s = 4.743$	3 / 3 / 6

**Table 4. Data for DRO branch.**

$\Gamma$	$x(0)$	$\dot{y}(0)$	$T$	(C/B)-sign & Floquet multipliers	$\mu_{CZ}^p / \mu_{CZ}^s / \mu_{CZ}$
3.00429783	0.99502455	0.07670173	0.40998	(-/+ ) $\varphi_p = 5.862$ , (-/+ ) $\varphi_s = 5.894$	1 / 1 / 2
3.00156431	0.99037034	0.06224607	1.02778	(-/+ ) $\varphi_p = 5.245$ , (-/+ ) $\varphi_s = 5.406$	1 / 1 / 2
3.00101739	0.98833167	0.06026263	1.32856	(-/+ ) $\varphi_p = 4.973$ , (-/+ ) $\varphi_s = 5.216$	1 / 1 / 2
3.00060753	0.98623049	0.05949811	1.64998	(-/+ ) $\varphi_p = 4.712$ , (-/+ ) $\varphi_s = 5.050$	1 / 1 / 2
3.00054882	0.98587513	0.05946574	1.7052	(-/+ ) $\varphi_p = 4.670$ , (-/+ ) $\varphi_s = 5.026$	1 / 1 / 2
2.99962388	0.97762100	0.06369886	3	(-/+ ) $\varphi_p = 4.001$ , (-/+ ) $\varphi_s = 4.787$	1 / 1 / 2
2.99935885	0.97409965	0.06735824	3.5	(-/+ ) $\varphi_p = 3.987$ , (-/+ ) $\varphi_s = 4.863$	1 / 1 / 2
2.99908502	0.97038828	0.07212000	4	(-/+ ) $\varphi_p = 3.995$ , (-/+ ) $\varphi_s = 5.001$	1 / 1 / 2
2.99868251	0.96488658	0.08024713	4.6003	(-/+ ) $\varphi_p = 4.185$ , (-/+ ) $\varphi_s = 5.254$	1 / 1 / 2

**Table 5. Data for one branch bifurcation from 3rd cover of the LPO2-orbit. These spatial orbits are simply-symmetric w.r.t. the  $xz$ -plane and ends at collision. Its symmetric family is obtained by using the reflection at the  $xy$ -plane.**

$\Gamma$	$x(0)$	$z(0)$	$\dot{y}(0)$	$T$	(C/B)-sign & Floquet multipliers	$\mu_{CZ}$
3.00363027	1.01440084	0	0.01974709	4.86	(-/+ ) $\varphi_p^3 = 3.305$ , $\varphi_s^3 = 0$	14 $\rightarrow$ 16
3.00362881	1.01439256	0.00046114	0.01976648	4.87	(-/+ ) $\varphi_1 = 3.300$ , (-/+ ) $\varphi_2 = 6.281$	14
3.00359018	1.01415816	0.00242577	0.02031752	4.90	(-/+ ) $\varphi_1 = 3.208$ , (-/+ ) $\varphi_2 = 6.280$	14
3.00357914	1.01409052	0.00273476	0.02047842	4.91	(+/+) $\lambda = -1.05$ , (-/+ ) $\varphi = 6.278$	14
3.00354287	1.01386628	0.003555363	0.02101794	4.94	(+/+) $\lambda = -1.18$ , (-/+ ) $\varphi = 6.255$	14
3.00325974	1.01198527	0.00688259	0.02594794	5.2	(+/+) $\lambda = -1.62$ , (-/+ ) $\varphi = 5.963$	14
3.00298774	1.00985792	0.00824897	0.03258269	5.5	(+/-) $\varphi_1 = 2.566$ , (-/+ ) $\varphi_2 = 5.657$	14
3.00270453	1.00652898	0.00795347	0.04651756	5.85	(-/+ ) $\varphi_1 = 1.947$ , (-/+ ) $\varphi_2 = 5.978$	14
3.00264234	1.00560524	0.00778449	0.05051319	5.88	(+/+) $\lambda = -1.09$ , (-/+ ) $\varphi = 5.958$	14
3.00263168	1.00544296	0.00774780	0.05124733	5.88	(-/+ ) $\varphi_1 = 3.488$ , (-/+ ) $\varphi_2 = 5.937$	14
3.00260038	1.00454296	0.00720347	0.05686831	5.86	(-/+ ) $\varphi_1 = 4.662$ , (-/+ ) $\lambda = 1$	b-d
3.00260927	1.00399399	0.00658371	0.06201856	5.8	(-/+ ) $\varphi = 4.813$ , (+/+ ) $\lambda = 2.278$	15
3.00266582	1.00306075	0.00521508	0.07465765	5.6	(-/+ ) $\varphi = 4.443$ , (+/+ ) $\lambda = 3.660$	15
3.00278841	1.00150186	0.00269606	0.11584022	5	(-/+ ) $\varphi = 3.653$ , (+/+ ) $\lambda = 1.829$	15
3.00279353	1.00129733	0.00238127	0.12512611	4.9	(-/+ ) $\varphi_1 = 3.540$ , (-/+ ) $\lambda = 1$	b-d
3.00277937	1.00084704	0.00169978	0.15351993	4.66	(-/+ ) $\varphi_1 = 3.246$ , (-/+ ) $\varphi_2 = 5.702$	14

**Table 6. Data for one branch bifurcation from 3rd cover of the  $LPO2$ -orbit. This family ends at the 5th cover of the  $DRO$ -orbit. Since the  $CZ$ -index is constant, this family forms a bridge between the two underlying planar periodic orbits. Moreover, these spatial orbits are simply-symmetric w.r.t. the  $x$ -axis. Its symmetric family is obtained by using the reflection at the ecliptic.**

$\Gamma$	$x(0)$	$\dot{y}(0)$	$\dot{z}(0)$	$T$	( $C/B$ )-sign & Floquet multipliers	$\mu_{CZ}$
3.00363027	1.01440084	0.01974709	0	4.86	( $-/+$ ) $\varphi_p^3 = 3.305$ , $\varphi_s^3 = 0$	14 $\rightarrow$ 16
3.00351924	1.01408954	0.01928185	0.01342237	4.96	( $-/-$ ) $\lambda_1 = -1.24$ , ( $-/-$ ) $\lambda_2 = 1.09$	15
3.00321170	1.01314307	0.01799332	0.02676988	5.25	( $-/-$ ) $\lambda_1 = -1.62$ , ( $-/-$ ) $\lambda_2 = 1.45$	15
3.00302231	1.01246670	0.01723541	0.03300118	5.46	( $+/-$ ) $\varphi = 2.749$ , ( $-/-$ ) $\lambda = 1.78$	15
3.00273486	1.01099334	0.01657953	0.04285920	5.82	( $+/-$ ) $\varphi = 1.618$ , ( $-/-$ ) $\lambda = 1.55$	15
3.00270684	1.01077857	0.01644568	0.04412031	5.85	( $+/-$ ) $\varphi = 1.801$ , ( $-/-$ ) $\lambda = 1.40$	15
3.00266563	1.01548137	0.01548137	0.04575934	5.88	( $+/-$ ) $\varphi = 2.506$ , ( $-/-$ ) $\lambda = 1.35$	15
3.00243536	1.01068879	0.00516070	0.04995370	6	( $-/+$ ) $\varphi = 5.761$ , ( $-/-$ ) $\lambda = 8.52$	15
3.00204821	1.01119864	-0.01174966	0.05089250	6.24	( $-/+$ ) $\varphi = 5.965$ , ( $-/-$ ) $\lambda = 31.1$	15
3.00172312	1.01167768	-0.02457421	0.04793350	6.5	( $-/+$ ) $\varphi = 6.016$ , ( $-/-$ ) $\lambda = 30.0$	15
3.00147493	1.01207539	-0.03349482	0.04374826	6.75	( $-/+$ ) $\varphi = 6.070$ , ( $-/-$ ) $\lambda = 22.3$	15
3.00127220	1.01242785	-0.04020652	0.03910792	7	( $-/+$ ) $\varphi = 6.124$ , ( $-/-$ ) $\lambda = 15.2$	15
3.00096072	1.01304236	-0.04944170	0.02947258	7.5	( $-/+$ ) $\varphi = 6.201$ , ( $-/-$ ) $\lambda = 6.16$	15
3.00073221	1.01358551	-0.05528744	0.01932635	8	( $-/+$ ) $\varphi = 5.911$ , ( $-/-$ ) $\lambda = 1.14$	15
3.00055690	1.01409401	-0.05914769	0.00388381	8.5	( $-/+$ ) $\varphi = 4.550$ , ( $-/-$ ) $\lambda = 1.00$	15
3.00054882	1.01412064	-0.05930512	0	8.52	( $-/+$ ) $\varphi_p^5 = 4.500$ , $\varphi_s^5 = 0$	16 $\rightarrow$ 14

**Table 7. Data for one branch bifurcation from 3rd cover of the  $g$ - $LPO1$ -orbit. These spatial orbits are simply-symmetric w.r.t. the  $x$ -axis and they are connected to one branch bifurcation from the 3rd cover of the  $DPO$ -orbit via birth-death. Its symmetric family is obtained by using the reflection at the ecliptic.**

$\Gamma$	$x(0)$	$\dot{y}(0)$	$\dot{z}(0)$	$T$	( $C/B$ )-sign & Floquet multipliers	$\mu_{CZ}$
3.00365597	0.985579006	-0.01951876	0	4.79	( $-/+$ ) $\varphi_p^3 = 3.205$ , $\varphi_s^3 = 0$	14 $\rightarrow$ 16
3.00365338	0.98556744	-0.01945341	0.00182488	4.80	( $-/+$ ) $\varphi = 3.214$ , ( $-/-$ ) $\lambda = 1.001$	15
3.00363389	0.98561874	-0.01938011	0.00580611	4.82	( $-/-$ ) $\lambda_1 = -1.01$ , ( $-/-$ ) $\lambda_2 = 1.005$	15
3.00329911	0.98657072	-0.01815373	0.02416862	5.12	( $-/-$ ) $\lambda_1 = -1.54$ , ( $-/-$ ) $\lambda_2 = 1.378$	15
3.00314093	0.98708523	-0.01763006	0.02950246	5.30	( $-/-$ ) $\lambda_1 = -1.02$ , ( $-/-$ ) $\lambda_2 = 1.685$	15
3.00300399	0.98759083	-0.01727225	0.03377964	5.46	( $+/-$ ) $\varphi = 2.290$ , ( $-/-$ ) $\lambda = 1.977$	15
3.00281046	0.98856773	-0.01745284	0.04009001	5.73	( $+/-$ ) $\varphi = 0.976$ , ( $-/-$ ) $\lambda = 2.451$	15
3.00275889	0.98918471	-0.01885469	0.04265726	5.82	( $+/-$ ) $\varphi = 0.134$ , ( $-/-$ ) $\lambda = 4.422$	15
						<b>b-d</b>
3.00275823	0.98925887	-0.01917383	0.04284561	5.82	( $-/-$ ) $\lambda_1 = 1.041$ , ( $-/-$ ) $\lambda_2 = 5.013$	14
3.00276196	0.98939330	-0.01992825	0.04305515	5.83	( $-/-$ ) $\lambda_1 = 1.148$ , ( $-/-$ ) $\lambda_2 = 6.636$	14

**Table 8.** Data for one branch bifurcation from 3rd cover of the  $g$ - $LPO1$ -orbit These spatial orbits are simply-symmetric w.r.t. the  $xz$ -plane and they are connected to one branch bifurcation from the 3rd cover of the  $DPO$ -orbit via birth-death. Its symmetric family is obtained by using the reflection at the ecliptic.

$\Gamma$	$x(0)$	$z(0)$	$\dot{y}(0)$	$T$	( $C/B$ )-sign & Floquet multipliers	$\mu_{CZ}$
3.00365597	0.985579006	0	-0.01951876	4.79	$(-/+)$ $\varphi_p^3 = 3.205$ , $\varphi_s^3 = 0$	14 $\rightarrow$ 16
3.00365461	0.98556706	-0.00036219	-0.01947401	4.80	$(-/+)$ $\varphi_1 = 3.215$ , $(-/+)$ $\varphi_2 = 6.281$	14
3.00363389	0.98568597	-0.00175392	-0.01975974	4.82	$(+/+)$ $\lambda = -1.01$ , $(-/+)$ $\varphi = 6.277$	14
3.00360033	0.98588066	-0.00278699	-0.02023321	4.84	$(+/+)$ $\lambda = -1.12$ , $(-/+)$ $\varphi = 6.263$	14
3.00331461	0.98766211	-0.00655464	-0.02492170	5.11	$(+/+)$ $\lambda = -1.52$ , $(-/+)$ $\varphi = 5.978$	14
3.00314742	0.98883839	-0.00763969	-0.02842198	5.29	$(+/-)$ $\varphi_1 = 3.031$ , $(-/+)$ $\varphi_2 = 5.756$	14
3.00289637	0.99094696	-0.00836889	-0.03579903	5.61	$(+/-)$ $\varphi_1 = 1.373$ , $(-/+)$ $\varphi_2 = 5.309$	14
3.00285045	0.99142732	-0.00835072	-0.03776509	5.67	$0.376 \pm 0.570i$ , $0.806 \pm 1.221i$	14
3.00277633	0.99243798	-0.00805049	-0.04244268	5.78	$0.491 \pm 0.121i$ , $1.917 \pm 0.472i$	14
3.00277358	0.99249304	-0.00802039	-0.04284315	5.79	$(+/+)$ $\lambda_1 = 1.987$ , $(-/-)$ $\lambda_2 = 2.016$	14
3.00276770	0.993012244	-0.00750257	-0.04644237	5.82	$\lambda_1 = 1.000$ , $(-/-)$ $\lambda_2 = 7.181$	b-d

## REFERENCES

- [1] U. Frauenfelder and A. Moreno, “On GIT quotients of the symplectic group, stability and bifurcations of periodic orbits,” *Journal of Symplectic Geometry*, To appear.
- [2] R. Broucke, “Stability of periodic orbits in the elliptic, restricted three-body problem.,” *AIAA J.*, Vol. 7, 1003, 1969.
- [3] U. Frauenfelder, D. Koh, and A. Moreno, “Symplectic methods in the numerical search of orbits in real-life planetary systems,” 2023.
- [4] C. Aydın, “The Conley–Zehnder Indices of the spatial Hill three-body problem,” *Celest. Mech. Dyn. Astron.*, Vol. 135, No. 32, 2023, 10.1007/s10569-023-10134-7.
- [5] M. G. Kreĭn, “On the application of an algebraic proposition in the theory of matrices of monodromy,” *Uspĕhi Matem. Nauk (N.S.)*, Vol. 6, No. 1(41), 1951, pp. 171–177.
- [6] M. G. Kreĭn, “On the theory of entire matrix functions of exponential type,” *Ukrain. Mat. Žurnal*, Vol. 3, 1951, pp. 164–173.
- [7] J. Moser, “New aspects in the theory of stability of Hamiltonian systems,” *Comm. Pure Appl. Math.*, Vol. 11, 1958, pp. 81–114, 10.1002/cpa.3160110105.
- [8] C. Conley and E. Zehnder, “Morse-type index theory for flows and periodic solutions for Hamiltonian equations,” *Comm. Pure Appl. Math.*, Vol. 37, No. 2, 1984, pp. 207–253, 10.1002/cpa.3160370204.
- [9] J. Robbin and D. Salamon, “The Maslov index for paths,” *Topology*, Vol. 32, No. 4, 1993, pp. 827–844, 10.1016/0040-9383(93)90052-W.
- [10] U. Frauenfelder and A. Moreno, “On doubly symmetric periodic orbits,” *Celestial Mech. Dynam. Astronom.*, Vol. 135, No. 2, 2023, pp. Paper No. 20, 18, 10.1007/s10569-023-10135-6.
- [11] C. Aydın, “The linear symmetries of Hill’s lunar problem,” *Arch. Math. (Basel)*, Vol. 120, No. 3, 2023, pp. 321–330, 10.1007/s00013-022-01822-1.
- [12] M. Hénon, “Numerical exploration of the restricted problem. V. Hill’s case: periodic orbits and their stability,” *Astr. Astrophys.*, Vol. 1, 1969, p. 223–238.
- [13] R. Restrepo and R. Russell, “A database of planar axi-symmetric periodic orbits for the solar system,” *AAS*, Vol. 17-694, 2017.
- [14] R. A. Dayung Koh and I. Bermejo-Moreno, “Cell-mapping Orbit Search for Mission Design at Ocean Worlds Using Parallel Computing,” Vol. 68, No. 172-196, 2021, 10.1007/s40295-021-00251-6.
- [15] V. Kalantonis, “Numerical Investigation for Periodic Orbits in the Hill Three-Body Problem,” *Universe*, Vol. 6(6), No. 72, 2020.